ISBN: 978-981-94-1156-6
2024 the 14th International Workshop on Computer Science and Engineering (WCSE 2024)
doi: 10.18178/wcse.2024.06.003

Retinal Neovascularization Localization in Optical Coherent Tomography Angiography Images Using Weighted Addition of Vessel Density and Bifurcation Density Maps

Yar Zar Tun and Pakinee Aimmanee +

School of Information Computer and Communication Technology, Sirindhorn International Institute of Technology, Thammasat University, Pathum Thani, Thailand

Abstract. Retinal neovascularization (RNV) is a pathological condition characterized by the abnormal growth of new blood vessels within the retina. Detecting RNV can be achieved through optical coherence tomography angiography (OCTA), an advanced imaging technology capable of visualizing retinal blood vessels. However, identifying RNVs within OCTA images is particularly challenging due to their varying patterns and sizes and overlapping vascular networks. In this study, we addressed this challenge by extracting features related to vessel density and bifurcation points within the vascular networks to pinpoint regions of interest (ROIs). Our systematic approach led to selecting a single ROI as the RNV region, with its maximum weighted addition of vessel and bifurcation densities as the location for RNV detection. Notably, our method achieved a localization accuracy of 68.29% in the 41 OCTA images with RNV, demonstrating a significant 14.63% improvement in performance over VNet-based localization.

Keywords: Retinal Neovascularization, RNV, Optical Coherent Tomography Angiography, OCTA, feature maps

1. Introduction

Optical coherence tomography angiography (OCTA) is a non-invasive imaging technique that offers detailed, depth-specific information about blood flow within the retinal and choroidal blood vessels [1]. It achieves this by analyzing the stability and fluctuations in backscattered light to detect the motion of blood cells in each layer of the retinal cross-section. Due to its continuous advancements, OCTA has emerged as an indispensable diagnostic tool for various retinal and choroidal disorders, including diabetic retinopathy and age-related macular degeneration. These conditions manifest with various clinical signs such as haemorrhage, exudates, and neovascularization (NV). OCTA has proven to be a superior and reliable method for efficiently visualizing and evaluating neovascular lesions compared to other retinal imaging techniques [2-4].

NV lesions in the retina are categorized into two main types based on their location within the retinal layers: choroidal neovascularization (CNV) and retinal neovascularization (RNV). CNV is primarily associated with age-related macular degeneration (AMD) and typically develops in the choriocapillaris and choroidal layers, protruding occasionally into intraretinal layers. In contrast, RNV is predominantly linked to diabetic retinopathy (DR) and typically originates in the retinal layer, extending into the vitreous cavity.

In this study, our primary focus centers on detecting RNV within OCTA images. Detecting RNV complexes poses a more significant challenge than choroidal neovascularization (CNV) due to their resemblance to the complex background of retinal vascular networks. RNV complexes exhibit a broad spectrum of patterns and sizes, ranging from tiny nodular knots and capillary loop fronds in their early stages [5]. As RNV matures, it can evolve into more intricate configurations, including medusa-like or tangled wool-like patterns, tight knots, beehive-like structures, or extensive networks of thick, matured vessels [6-7]. For visual reference, please refer to Fig. 1, which showcases examples of these various RNV patterns.

+ Corresponding author. Tel.: 02-501-3505 ext 5012.
E-mail address: pakinee@siit.tu.ac.th.

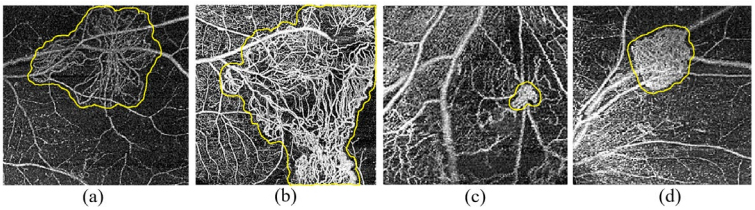

Fig. 1: Examples of RNV patterns: (a) medusa, (b) oversized frond/ tangled wools, (c) a knot, and (d) beehive.

2. Literature Review

Research on automatic neovascularization (NV) analysis using OCTA images began in 2015. Most studies in this field have primarily focused on the automatic detection, segmentation, and quantification of NV related to the choroidal neovascularization (CNV) type [8].

The number of works related to the automatic analysis of RNV is significantly lower than those focused on CNV, primarily because RNV presents more challenging research problems. Most of the work related to RNV involved clinical studies [8]. The following are only studies on RNV segmentation and quantification on OCTA images. All were published between 2021 and 2022.

In RNV segmentation, Wu et al. [9] conducted the initial study in 2021 employing image processing techniques. Their approach involved partial line detection and the vascular connectivity algorithm, composed of colour space conversion, pixel clustering, artefact removal, and OTSU's binarization [10] to effectively segment RNV vessels within OCTA images of the vitreous layer. In a subsequent study by Li et al. [11], ResNet 101 [12] was utilized to identify the presence of RNV in Ultra-wide OCTA (UW-OCTA) images of the superficial retinal layer. Subsequently, the RNV images were input into VNet [13] to segment the RNV lesions precisely.

This paper introduces a novel approach for pinpointing an RNV location in OCTA images using feature maps derived from vessel density and bifurcation points. We achieved a localization accuracy of 68.29%, a substantial enhancement compared to the state-of-the-art method, including the VNet-based method, VNet_Li [11], with an improvement of 14.63%. Notably, this technique represents a pioneering endeavour in RNV localization, significantly contributing to automated RNV analysis within the research community.

3. Methodology

Our proposed algorithm comprised five steps: preprocessing, vessel detection, vessel feature density maps generation, strength map generation, and localization of the RNV region. Fig. 2 depicts our framework.

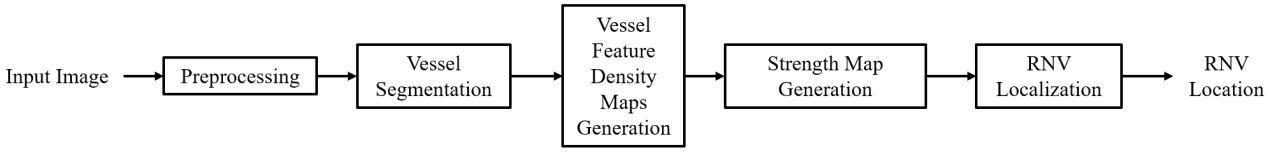

Fig. 2: Overall method's framework.

The details of each step are described in the following subsections.

3.1. Preprocessing

To enhance contrast in the input image, which was affected by noise and resulted in low contrast between foreground and background pixels, we utilized a selective linear mapping technique [14]. This method adjusts intensity values, rounding up the top 20% to the maximum intensity and rounding down the bottom 20% to the minimum intensity.

3.2. Vessel Segmentation

Blood vessels of varying sizes naturally exist in the superficial retinal layers of OCTA images. We employed the Frangi filter [15] to solve the multiple-vessel sizing problem. Our vessel segmentation process was divided into three channels for three vessel sizes. Gaussian filtering with smoothing parameters of 1.5,

2.5, and 1.75, Frangi sensitivity 25, 15, and 5, and Gaussian kernels with standard deviations 38-42, 11-15, and 1-11 in the Frangi's Hessian matrix, were used for large, medium, and small size vessels, respectively.

Niblack thresholding [17] improved the visibility of vessels detected in Frangi's results. Equation (1) illustrates the Niblack thresholding (T) applied to a small square window centered at (x, y).

$$T(x, y) = \mu(x, y) + k.\beta(x, y), \tag{1}$$

where $\mu(x, y)$ is the average intensity, $\beta(x, y)$ is the intensity's standard deviation, and k is a constant. We used window widths of 96, 32, and 8 pixels, and k of 1.2, 0.7, and 0.7, for the large to small channels, respectively. Morphological closing [18], employing a disk-shaped structuring element, was used to seal small undesired gaps at vessel branching points and within the vessels. Specifically, disk elements with radii of 5, 2, and 2 pixels were utilized in the three channels. Finally, the vessel networks obtained from each channel were combined to represent the entire vessel network comprehensively.

3.3. Vessel Feature Density Maps Generation

A vessel density map and a bifurcation density map were considered. First, a medial surface axis thinning algorithm [19] was employed to derive a skeleton of the vessel network. This algorithm progressively reduced the thickness of foreground objects within the binary image to one pixel, preserving the original object's topology and connectivity. To produce a vessel density map D_v, we utilized a moving window filter [20] with dimensions of 21×21 pixels and a step size of one pixel applied to the skeleton image. The vessel density at a point (x, y) is a ratio of the number of vessel pixels to the total area in the moving window centering the point.

A bifurcation points image was generated from the vessel skeleton image using neighborhood analysis, connectivity assessment, and morphological operations. Points connected to three or more neighbors were marked as bifurcation points. Iterative morphological operations removed false positives. To get a bifurcation density map D_v, a moving square window of widths 21 pixels [20] and a step size of one pixel was used. The bifurcation density was then calculated by finding the ratio of bifurcation points to the total area within the window. Fig. 3 depicts the skeleton image, the vessel density map, the vessel bifurcation points image, and the vessel bifurcation density maps.

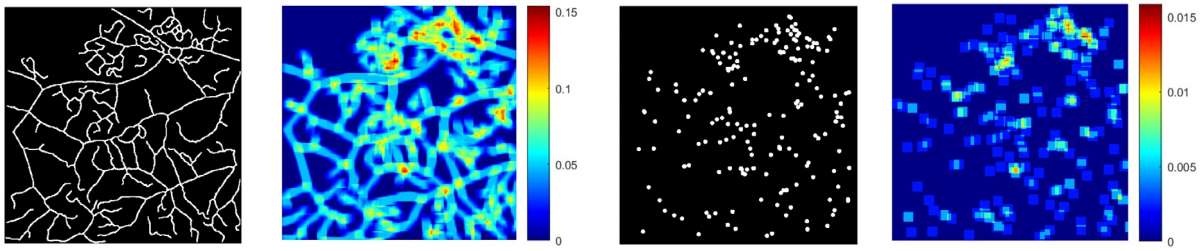

Fig. 3: Illustration of vessel feature density maps creation- skeleton vessels (first), vessel density map (second), a vessel bifurcation points map (third), and a vessel bifurcation density map (fourth)

3.4. Strength Map Generations

Strength map (S) depicting locations in the image that potentially contain RNV were used for determining the RNV location. Min-max normalization [21] was applied to the density maps D_v and D_b to equalize the ranges in both maps. The following four strength maps: S_V, S_B, S_{EM}, and S_{WA} were used.

a. S_V is the same as the normalized vessel density map D_v
b. S_B is the same as the normalized vessel bifurcation density map D_b
c. S_{EM} is the result of elementwise multiplication of normalized D_v and D_b
d. S_{WA} is the result of the weighted addition of normalized D_v and D_b with the weights set to the accuracies of the RNV localization using S_V and S_B

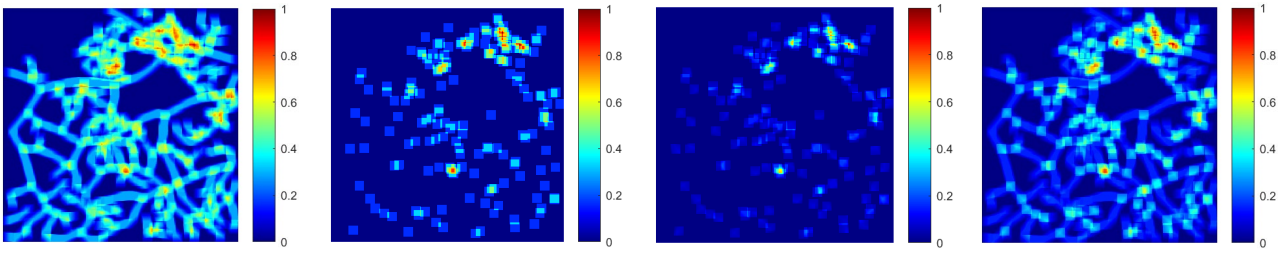

(a) S_V (b) S_B (c) S_{EM} (d) S_{WA}

Fig. 4: Illustration of four strength maps

3.5. Localization of the RNV Region

We used a strength map to determine the RNV location. The values in the strength map that are above the 75th percentile were considered for the candidate regions. Among the candidate regions, the largest cluster was the region of interest, R. The location Loc of RNV, was where the strength value, S is maximum within R. The localization process is mathematically defined as in equation (2). Fig. 5 shows candidate regions and the predicted RNV location.

$$Loc = \arg\max S(x, y) \text{ for all } (x, y) \in R \tag{2}$$

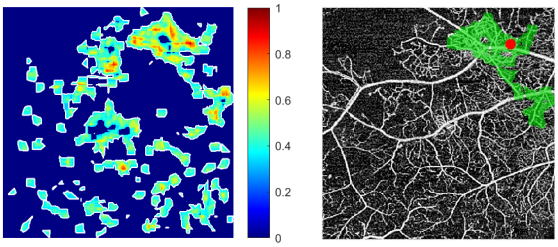

Fig. 5: Illustration of candidate regions (left) and an RNV location (red dot) on the green largest candidate region (right).

The result was considered successful when the RNV location lies within or on the ground truth's boundary. The accuracy, the ratio of correct localization to the total number of images, is used for evaluation.

4. Experiment and Result

We used 41 SS-OCTA [5] images, each 6 mm square in width, capturing RNV at superficial retinal layers sourced from Thammasat University Hospital in Thailand. The ground truth images were hand-drawn by experts. We compared our proposed method against a deep learning-based approach (VNet_Li) [11]. For convenience, we named our method *Strength-Map-based Localization (SML)*. Four variances of SML from four different maps are compared. Fig. 6 illustrates examples of successful localization, and Table 1 depicts the accuracy comparison of the RNV localization using four strength maps.

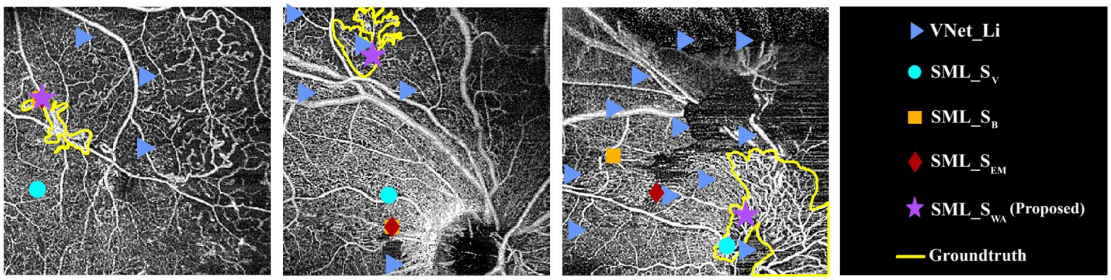

Fig. 6: Examples of localization results from SML based on different strength maps against a comparative method VNet_Li.

Table 1: Comparison of RNV localization accuracies from different methods

Methods	**VNet_Li [11]**	**SML based on**			
		S_V	S_B	S_{EM}	S_{WA} **(Proposed)**
Accuracy (%)	53.66	63.41	65.85	65.85	**68.29**

Fig. 6 depicts localization from different methods. Notably, the VNet_Li, one of the comparative methods, tends to over-segment, resulting in multiple false locations. The proposed SML based on S_{WA} map yielded the highest accuracy compared to other strength maps. The accuracy improvements of SML based on S_{WA} over VNet_Li [11], and SML based on S_V, S_B, and S_{EM} were 14.63%, 4.88%, 2.44%, and 2.44%. The failed cases were analyzed and found to be caused by undetectable vessels in dense RNV and misinterpretation of similar vessels. Our future work will find efficient vessel detection and noise removal algorithms and consider more features, such as vessel thinness and proximity to ischemic areas [2].

5. Conclusion

We've devised an innovative method to precisely locate Retinal Neovascularization (RNV) in superficial retinal OCTA images. Our approach combines vessel density and bifurcation density through weighted addition, outperforming individual use, elementwise multiplication, and VNet-based localization [11]. This method achieves a localization accuracy of 68.29%. However, further algorithm refinement including improving vessel segmentation and candidate region selection and considering other RNV biomarkers.

6. Acknowledgement

This project was financially funded by the National Research Council of Thailand under grant number NRCT5-RSA63010-05 and Center of Excellence in Biomedical Engineering at Thammasat University.

7. References

[1] R. F. Spaide, J. G. Fujimoto, N. K. Waheed, S. R. Sadda, and G. Staurenghi. Optical coherence tomography angiography. *Prog. Retin. Eye Res.* 2018, 64: 1–55.

[2] J. P. Ehlers, Y. Modi, S. K. Srivastava, and P. K. Kaiser, *OCT and OCTA in retinal disorders.* Wolters Kluwer, 2021.

[3] M. Menean, R. Sacconi, B. Tombolini, F. Federico, F. Bandello, and G. Querques. Combined Wide-Field Imaging in Grading Diabetic Retinopathy. *Eye* 2023, 38(1), 210–214.

[4] B. N. Vofo, P. Galarza, I. Chowers, and J. Levy. Interest of widefield-optical coherence tomography angiography for diagnosis and follow-up of retinal neovascularisation in proliferative diabetic retinopathy. *J. Ophthalmol.* 2022, 2022, 5746238.

[5] J. Yang, and Y. Chen. Diabetic Retinopathy. In: M. Zofia, et al (eds.). *Scientific and Technical Documentation Press.* Springer, 2023.

[6] S. Vaz-Pereira, J. J. Silva, K. B. Freund, and M. Engelbert. Optical coherence tomography angiography features of neovascularization in proliferative diabetic retinopathy. *Clin. Ophthalmol.* 2020, 14: 3351–3362.

[7] C. J. Ong, M. Y. Wong, K. X. Cheong, J. Zhao, K. Y. Teo and T. -E. Tan. Optical coherence tomography angiography in retinal vascular disorders. *Diagnostics* 2023, 13(9): 1620.

[8] Y.Z. Tun, P. Aimmanee. A Complete Review of Automatic Detection, Segmentation, and Quantification of Neovascularization in Optical Coherence Tomography Angiography Images. Diagnostics 2023, 13, 3407. https://doi.org/10.3390/diagnostics13223407

[9] S. Wu, S. Wu, H. Feng, Z. Hu, Y. Xie, Y. Su, T. Feng, and L. Li. An optimized segmentation and quantification approach in microvascular imaging for OCTA-based neovascular regression monitoring. *BMC Med. Imaging* 2021, 21(1): 13.

[10] N. Otsu. A threshold selection method from gray-level histograms. *IEEE Trans. Syst. Man Cybern.* 1979, 9(1): 62–66.

[11] Y. Li, R. Zeghlache, I. Brahim, H. Xu, Y. Tan, P. -H. Conze, M. Lamard, G. Quellec, and M. El Habib Daho. Segmentation, classification, and quality assessment of UW-octa images for diagnosis of diabetic retinopathy. In: B. Sheng, et al (eds.). Proc. Of Mitosis Domain Generalization and Diabetic Retinopathy Analysis. MIDOG DRAC 2022 2022. Lecture Notes in Computer Science, vol 13597. Springer, Cham. 2022.

[12] K. He, X. Zhang, S. Ren and J. Sun. Deep Residual Learning for Image Recognition. In: *Proc. Of IEEE Conf. Comput. Vis. Pattern Recognit. (CVPR).* Las Vegas: IEEE Computer Society. 2016, pp. 770-778.

[13] F. Milletari, N. Navab, S. -A. Ahmadi. V-net: Fully convolutional neural networks for volumetric medical image segmentation. In: *Proc. of Int. Conf. 3D Vis..* Stanford: IEEE Computer Society. 2016, pp. 565-571.

[14] R. C. Gonzalez, and R. E. Woods. *Digital Image Processing*. Pearson, 2008.

[15] A. F. Frangi, W. J. Niessen, K. L. Vincken, M. A. Viergever. Multiscale vessel enhancement filtering. In: W. M. Wells, et al (eds.). Medical Image Computing and Computer-Assisted Intervention. MICCAI'98. MICCAI 1998. Lecture Notes in Computer Science. Springer. 1998.

[16] L. G. Shapiro, and G. C. Stockman. *Computer Vision*. Prentence Hall, 2001.

[17] W. Niblack. *An Introduction to Digital Image Processing*. Prentice Hall, 1986.

[18] E. R. Davies. *Computer and machine vision: Theory, algorithms, practicalities.* Academic, 2012.

[19] T. C. Lee, R. L. Kashyap, and C. N. Chu. Building skeleton models via 3-d medial surface axis thinning algorithms. *CVGIP: Graphical Models and Image Processing 1994*, *56*(6): 462–478.

[20] C. K. Ko. Analysis of sliding window techniques for exponentiation. *Comput. Math Appl.* 1995, 30(10): 17-24.

[21] J. Han, J. Pei, and M. Kamber. Data Preprocessing. Morgan Kaufmann, 2011.